Biophysical Journal
Article

Biophysical Society

Nonuniform filament turnover, contractility, and bundle formation in disordered actomyosin networks

Alexander K. Y. Tam,[1,*] Alex Mogilner,[2,*] and Dietmar B. Oelz[3]
[1]UniSA STEM, The University of South Australia, Mawson Lakes, South Australia, Australia; [2]Courant Institute of Mathematical Sciences, New York University, New York, New York; and [3]School of Mathematics and Physics, The University of Queensland, St Lucia, Queensland, Australia

ABSTRACT We use mathematical modeling and simulation to investigate how filament turnover and mechanics influence contractility and bundle formation in disordered actomyosin networks. Using a two-dimensional agent-based model for an actomyosin network, we investigate four simplified models for filament turnover: uniform, biased, branching, and treadmilling. With no turnover, over time contractility decreases and bundle formation increases, and networks eventually form stationary patterns that cannot contract. Introducing turnover allows contractility to persist longer compared with the no-turnover scenario. Uniform turnover, where new filaments have random positions and orientations, disrupts bundle formation and enables persistent contractility. In biased turnover, branching, and treadmilling, the positions and orientations of new filaments depend on the existing network. These nonuniform turnover models increase bundle formation compared with uniform turnover, while still allowing long-term contractility. Branching at 70° disrupts bundle formation to enable prolonged contractility, whereas filament treadmilling disrupts the trade-off between bundle formation and contractility. Biased turnover places new filaments near existing ones, which promotes bundle formation but is less effective at maintaining contractility. Simulations showed that more bendable filaments accelerate bundle formation, while higher effective cross-linking friction enhances contractility. Our results suggest that cells can tune contractility and bundle formation in disordered actomyosin networks by varying actin turnover pathways.

SIGNIFICANCE In muscle cells, crystal-like actin-myosin arrays generate contractions by a well-known mechanism. Disordered actomyosin networks of nonmuscle cells are also able to contract, but the respective mechanisms are much less understood. One of the main factors affecting this disordered contractility is actin filament turnover. We use mathematical modeling to investigate how different modes of actin turnover influence contractility and bundle formation. Without turnover, actomyosin networks form patterns that lose contractility. Uniform and branching turnovers disrupt bundle formation, enabling persistent contractility. Actin treadmilling disrupts the trade-off between bundle formation and contractility, whereas spatially biased turnover hastens bundle formation, inhibiting long-term contractility. Our study leads to mechanistic understanding of how different modes of actin turnover affect network bundling and actomyosin contractility.

INTRODUCTION

The actin cytoskeleton is a dynamic network of actin filaments (F-actin) and actin-binding proteins shaping cells (1). Interactions between F-actin and clusters of myosin-II motors form actomyosin networks, which generate the mechanical forces enabling cell movement and division (1–3). Actin filaments, with lengths on the micron scale (4–6), are polar, with distinct plus and minus ends. Myosin motor clusters bind to F-actin filament pairs and generate force and movement toward filament plus ends (7). Actin filaments are also interconnected by dynamic cross-linker proteins that restrict relative motion between filaments, but do not move actively along them (8). These actions generate dynamic and contractile actomyosin networks (9–12). Throughout this work, we will refer to actin filaments (F-actin) as filaments, and myosin-II motor clusters as motors.

In muscles, filaments form linear arrays called sarcomeres where filaments and motors are arranged in a perfect

Submitted November 19, 2025, and accepted for publication February 20, 2026.

*Correspondence: alexander.tam@adelaide.edu.au or mogilner@cims.nyu.edu

Editor: Guy Genin.
https://doi.org/10.1016/j.bpj.2026.02.032

crystalline order (13), enabling contraction by the well-understood sliding filament mechanism (7,13). However, sarcomeric structure is not a necessary condition for actomyosin contraction: in nonmuscle cells, filaments are oriented and distributed with much less order. Here, we will not discuss force generation in stress fibers, ubiquitous in nonmuscle cells (14,15) but sharing some features similar to sarcomeric structures in muscle cells (16). Instead, we will focus on the problem of the actomyosin contraction in disordered networks of the kind characteristic for the cell cortex (3,17,18).

Modeling and simulation have been used to investigate actomyosin contraction (12,17,19–34). Relevant agent-based models include the publicly available software Cytosim (35), AFINES (36), and MEDYAN (37). These studies have shown that actomyosin contractility depends on factors including filament geometry (17,27,29), bending (18,23) and buckling (30,32), protein friction (18,23), cross-linking (22,26), delayed myosin unbinding (19), drag forces (23), and filament treadmilling (12). Other studies have focused on bundle formation in actomyosin networks (38–41). Cross-linking (42–45) has been shown to be the key for bundle formation in networks without myosin. Recent computational studies of bundle formation in actomyosin networks have demonstrated how cross-linking (37,40,46–48), initial orientation (47,49,50), motor density (47,49,51), kinetics (52), and treadmilling (47,49) affect bundle formation.

Some of these models showed, in particular, that filament turnover (dynamic assembly and disassembly) disrupts more stationary patterns, such as bundles, forming in the networks (53), and leads to prolonged contractility (6,18,48,54,55). In cells, specialized mechanisms regulate various modes and rates of filament turnover (56). We condense these complex molecular mechanisms into four simplified turnover models: uniform, biased, branching, and treadmilling. In uniform turnover, newly recruited filaments have random positions and orientations. Unlike uniform turnover, in biased, branching, and treadmilling turnover the positions and orientations of new filaments depend on the existing network architecture.

In this article, we investigate how mechanics and filament turnover affect contractility and bundle formation in disordered actomyosin networks. We adapt the mechanical model for filaments and motors of (23) and simulate network evolution with four different models of filament turnover: uniform, biased, branching, or treadmilling. We quantify contractility and bundling, and then vary turnover rates, modes to investigate their effects on contractility and bundle formation. Without turnover, filaments form stationary bundles that lose contractility. In general, nonuniform turnover increases bundle formation compared with uniform turnover, while still enabling persistent contractility. Branching prolongs contractility by disrupting bundle formation, whereas treadmilling lessens the trade-off between bundle formation and contractility. Mechanical factors, especially filament flexibility and protein friction, also promote contractility and bundle formation.

MATERIALS AND METHODS

We use a two-dimensional (2D) agent-based model to investigate how turnover and mechanics influence actomyosin bundle formation. We simulate the model using code written in Julia, quantifying both network contractility and bundle formation.

Mechanical model

We represent filaments as chains of nodes connected by stiff linear springs, each spring having the same equilibrium length (23,29). Filaments are semiflexible (57), and experience small-but-significant bending deformation. We represent motors as two nodes (motor domains) connected by a spring with zero equilibrium length (23,29). Motors attach to filament pairs at their intersection, and each node moves toward the plus end of the attached filament according to a linear force-velocity relationship (58) (see Fig. 1 *B*). The degrees of freedom of our model are the vector-valued filament node positions, and the relative positions of motors along the filaments.

We do not explicitly model the movement of unattached motors or motors attached to a single filament. Instead, we remove motors from the network at a rate given by Bell's law (59) to simulate force-dependent unbinding, and also remove a motor if either motor domain reaches the plus end of a filament. When a motor is removed, we immediately replace the removed motor with a new motor located at an intersection between a pair of filaments. We select the filament-filament intersection at which to place the new motor randomly. While this approximation is relatively restrictive, our approach to motor binding and unbinding ensures that the number of motors remains constant at all times during the simulation.

Our model includes protein friction at all intersections between pairs of filaments that do not have an attached motor. We model protein friction as a pointwise viscous drag that penalizes relative motion between two intersecting filaments at their intersection. In practice, protein friction might represent cross-linking of a filament pairs (10), or contact-like forces between two filaments (60). Protein-friction forces are larger than hydrodynamic friction between filaments and the cytoplasm, and have similar magnitude to forces exerted by motors (60). Schematics of the filaments, motors, their interactions, and the relevant mechanical forces are illustrated in Fig. 1, *A* and *B*.

We express our mechanical model as the system of force-balance equations,

$$0 = \boldsymbol{F}_{\mathrm{a,\ drag}} - \delta E_{\mathrm{a,\ bend}} - \delta E_{\mathrm{a,\ spring}} + \boldsymbol{F}_{\mathrm{a,\ pf}} - \delta E_{\mathrm{m,\ spring}} + \boldsymbol{F}_{\mathrm{m,a}}. \tag{1}$$

The first four terms on the right-hand side of (1) are the mechanical contributions of the filaments. The symbol $\boldsymbol{F}_{\mathrm{a,\ drag}}$ represents viscous drag between the filaments and the cytoplasm. The filament bending force is the variation of the filament bending energy $E_{\mathrm{a,\ bend}}$, where $E_{\mathrm{a,\ bend}}$ integrates elastic potential energy along the filament length. The variation of $E_{\mathrm{a,\ spring}}$ is the sum of spring forces for each segment between adjacent nodes of a filament. We assume that each spring satisfies Hooke's law, with spring constant k_{a}. Since filaments are effectively inextensible (61), we assume a large value of spring stiffness, $k_{\mathrm{a}} = 1000\ \mathrm{pN}\mu\mathrm{m}^{-1}$, for every filament segment. The symbol $\boldsymbol{F}_{\mathrm{a,\ pf}}$ represents viscous drag forces due to protein friction. These forces apply pointwise at intersections between filaments, and penalize relative motion of the intersecting filaments.

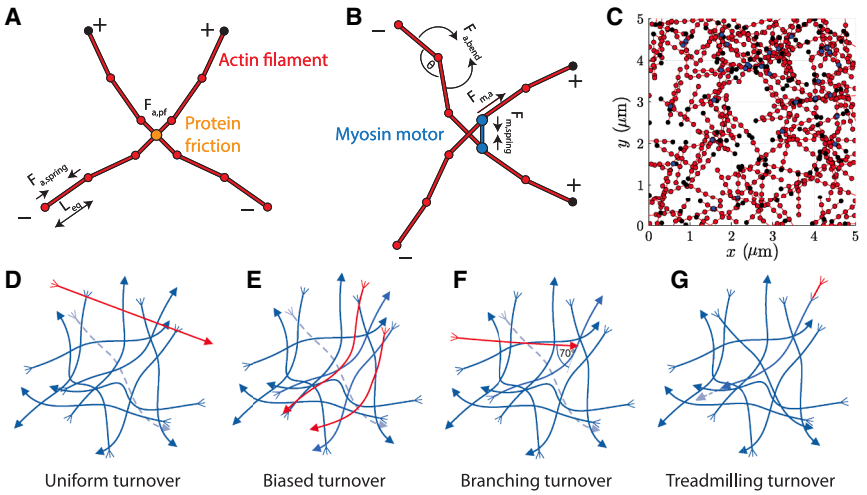

FIGURE 1 (*A* and *B*) Schematic of filaments, motors, and their interactions, and mechanical features included in the model. (*C*) Example of a random initial condition used in the simulations. (*D–G*) Illustration of the different models for filament turnover considered in this study. In each sketch, dark blue curves represent filaments (*arrows* indicate minus ends and *tridents* indicate plus ends). Dashed curves illustrate the random selection and removal of a filament from the network, and red curves represent newly added filaments due to turnover. Where appropriate, light blue filaments represent a reference filament on which the newly added filament is based. (*D*) Uniform turnover, where the new filament has random position and orientation and zero curvature. (*E*) Biased turnover, where the new filament is a copy of an existing filament, with a translation and rotation, and sometimes polarity reversal. (*F*) Branching turnover, in which new filaments appear at an angle of 70° to existing filaments. (*G*) Treadmilling turnover, where a filament depolymerizes (shrinks) at its minus end and polymerizes (grows) at its plus end.

The final two terms on the right-hand side of (1) are mechanical contributions from motors. We represent motor-stretching forces as the variation of spring energy $E_{\mathrm{m,\ spring}}$. Like filaments, we assume that a spring satisfying Hooke's law connects the two motor nodes. We assume this spring to be stiff, with spring constant $k_{\mathrm{m}} = 1000\ \mathrm{pN}\mu\mathrm{m}^{-1}$, to maintain a motor length close to zero throughout the simulation. The final force term, $\boldsymbol{F}_{\mathrm{m,a}}$, models filament-motor interactions, for which we adopt a linear force-velocity relationship. Like the model of (23), we neglect thermal forces, which can accelerate bundle formation but do not affect the eventual morphology (42).

Turnover models: Uniform, biased, branching, and treadmilling

Turnover refers to the continuous exchange of network components between the network and cytoplasm (6). To maintain the total number of filaments throughout a simulation, we implement the simplified representation of filament turnover by removing a filament (and any motors attached to the filament) from the network with certain rate, and immediately replacing the removed filament (and motor, if applicable) with a new one. This is often a realistic scenario, as the ends of the filaments are usually capped for some time, after which these filaments are rapidly disassembled by severing (62,63). Similarly, filament addition can be considered instant, as the duration of filament growth after nucleation is often much shorter than the time interval after the end capping, before the disassembly starts (62). Models often consider actin turnover whereby the position and orientation of new filaments is random (6,18,23). However, both filament disassembly and nucleation rates depend on the concentrations of several types of actin-binding proteins (62,64,65) that are not uniformly distributed in space, so filament turnover could exhibit spatial bias. Indeed, turnover often involves a polarized flux of actin toward specific regions in the cell, indicating spatial nonuniformity (56).

We implement four turnover models: uniform, biased, branching, and treadmilling turnover. Regardless of turnover model, we assume that filaments undergo turnover with constant rate $k_{\mathrm{off},a}$, same for every filament. The probability that a filament turns over in one time step of the simulation is then $P_{\mathrm{turnover}} = 1 - \mathrm{e}^{-k_{\mathrm{off},a}\Delta t}$, where Δt is the time step size. In uniform turnover, new filaments have zero curvature, and have positions and orientations chosen at random from uniform distributions (see Fig. 1 *D*). In contrast, the existing network architecture influences the positions and orientations of new filaments in biased, branching, and treadmilling turnover.

Biased turnover (Fig. 1 *E*) captures a tendency for new filaments to form close to existing ones, for example, due to the nucleating factor associating with existent filaments. In biased turnover, after removing a filament we introduce the new one by first copying an existing reference filament selected at random from those remaining in the network. We then rotate the newly copied filament about its center, by a normally distributed random angle $\theta \sim \mathcal{N}(0, \sigma_{t,\theta}^2)$, and translate the rotated filament by a vector $\boldsymbol{x} \in \mathbb{R}^2 = (x, y) \sim (\mathcal{N}(0, \sigma_{t,x}^2), \mathcal{N}(0, \sigma_{t,y}^2))$, where $\boldsymbol{x}$ is dimensionless and scaled by domain width. The standard deviations $\sigma_{t,\theta}$, $\sigma_{t,x}$, and $\sigma_{t,y}$ are model parameters. Smaller standard deviations result in stronger bias. When implementing biased turnover, we also swap the plus end and minus end of the new filament with probability P_{rev}. In typical simulations, we set $P_{\mathrm{rev}} = 0.5$. Reversing the filament polarity mimics the observation that plus ends and minus ends alternate in stress fibers (14).

Filament branching mediated by the Arp2/3 complex (66) is another turnover scenario. Arp2/3 stimulates nucleation of new daughter filaments that grow at an angle of $70 \pm 7°$ from the side of the mother filament (66). To implement branching, we remove a filament from the network and introduce a new filament with zero curvature whose minus end coincides with a random position along a randomly selected existent filament. The new filament is oriented at a θ_b degree angle from the relevant segment of the reference filament. We simulate networks with different values of θ_b, but $\theta_b = 70°$ corresponds to Arp2/3-mediated branching. Branching turnover is illustrated in Fig. 1 *F*.

Treadmilling represents actin filament remodeling by simultaneous plus end polymerization and minus end depolymerization (62,67–69). To implement treadmilling, we remove the filament segment closest to the minus end, and add a new segment to the filament at the plus end (Fig. 1 *G*). We assume that new segments have the equilibrium segment length and the same orientation as the adjacent segment.

Numerical methods

We implement the model in a spatially 2D simulation environment written in Julia. Our code simulates network evolution using discrete, equispaced time steps. In each time step, we first simulate filament turnover and motor binding and unbinding. We then solve the force-balance equation (1) to implement the mechanical component of the model. We solve the mechanical model by obtaining the filament and motor positions that minimize the functional

$$E := E_{\text{a, drag}} + E_{\text{a, bend}} + E_{\text{a, spring}} + E_{\text{a, pf}} + E_{\text{m, spring}} + E_{\text{m,a}}. \quad (2)$$

Each term in Eq. (2) corresponds to a term in the force-balance equation (1). The symbols $E_{\text{a, drag}}$, $E_{\text{a, pf}}$, and $E_{\text{m,a}}$ denote terms whose variations are finite-difference approximations of the forces $\boldsymbol{F}_{\text{a, drag}}$, $\boldsymbol{F}_{\text{a, pf}}$, and $\boldsymbol{F}_{\text{m,a}}$, respectively, which we interpret as dissipative energies in the context of Onsager's variational principle (70). The mathematical forms for the energy terms in Eq. (2) are included in the supporting material. In Julia, we minimize the energy functional equation (2) using the limited-memory Broyden-Fletcher-Goldfarb-Shanno method (71–74), using the Optim.jl package (75).

Quantifying contractility

In our simulations, we assume that filament motion gives rise to uniform elongation and shearing of the 2D domain in which the network resides. This assumption neglects the details of where forces are propagated through the network and their direction, and is common in actomyosin network simulations (5,6,12,23). Uniform deformation would occur for a dense network with numerous overlapping copies of the reference network of simulated filaments (see the supporting material for an illustration). Such a dense network is a reasonable approximation of a real network. Under the assumption of uniform deformation in the domain, we can associate the forces occurring within the domain with uniform forces at the boundaries. We can then quantify contractility by viewing the domain as a simple plane stress element. We discuss this scenario further in the context of a two-filament motor assembly in (29).

For uniform elongation and shear, we can use the energy minimization technique to compute the forces on the domain boundary. We define

$$E_{\text{tot}} := E + \boldsymbol{F}_x \cdot \boldsymbol{L}_x + \boldsymbol{F}_y \cdot \boldsymbol{L}_y, \quad (3)$$

where E is defined in Eq. (2), and $\boldsymbol{L}_x = (L_{xx}, L_{xy})$ and $\boldsymbol{L}_y = (L_{yx}, L_{yy})$ are vectors specifying two edges of the domain. The vectors $\boldsymbol{F}_x$ and $\boldsymbol{F}_y$ contain the normal and shear force components on the domain boundary. In numerical simulations with constant domain size and shape, unconstrained minimization of Eq. (3) is equivalent to minimizing Eq. (2), where the force vectors $\boldsymbol{F}_x$ and $\boldsymbol{F}_y$ are Lagrange multipliers that enforce the constant domain size constraints. In numerical simulations, at each time step we compute force components using

$$\boldsymbol{F}_x = -\partial_{\boldsymbol{L}_x} E, \quad \boldsymbol{F}_y = -\partial_{\boldsymbol{L}_y} E. \quad (4)$$

Neglecting possible out-of-plane stresses, the state of stress in the network is given by the 2d stress tensor

$$\boldsymbol{\sigma} = \begin{bmatrix} F_{xx}/L_{yy} & F_{xy}/L_{yy} \\ F_{yx}/L_{xx} & F_{yy}/L_{xx} \end{bmatrix}. \quad (5)$$

The mean normal stress,

$$\sigma = \frac{1}{2}\text{tr}(\boldsymbol{\sigma}) = \frac{\sigma_{xx} + \sigma_{yy}}{2}, \quad (6)$$

then provides a measure of instantaneous network contractility, and by convention negative σ indicates contraction, and positive σ indicates expansion. We also introduce the time-averaged mean normal stress,

$$\overline{\sigma} = \frac{1}{T}\int_0^T \sigma(t)\, \mathrm{d}t, \quad (7)$$

where T is the total simulation duration. The time-averaged mean normal stress $\overline{\sigma}$ is our primary measure to quantify the net expansion or contraction generated in simulated networks. Throughout this work, we denote all quantities averaged over time using bars.

Quantifying aggregation and bundle formation

We define three statistical indices to quantify aggregation and bundle formation. These indices,

$$I_a = \frac{N_a}{N_f(N_f - 1)/2}, \quad (8)$$

$$I_b = \frac{N_b}{N_f(N_f - 1)/2}, \quad (9)$$

$$I_p = \frac{N_p}{N_f(N_f - 1)/2}, \quad (10)$$

are the aggregation index, bundle index, and parallel-bundle index, respectively. All three indices are ratios of the number of a particular type of filament pair, to the total number of pairs in the network, $N_f(N_f - 1)/2$, where N_f is the total number of filaments. To compute the aggregation index Eq. (8), we count the number of filament pairs that are sufficiently close to each other, N_a. We assume that two filaments are sufficiently close if any node on one filament is within 0.25 μm of any node of the other filament. In the bundle index Eq. (9), N_b is the number of aligned close filament pairs in the network. A pair is included in N_b if the two filaments are sufficiently close, using the same definition as for N_a, and have similar orientation. We classify a filament pair as having similar orientation if the acute angle between any pair of sufficiently close segments is less than or equal to 20°. Finally, the count N_p for the parallel-bundle index Eq. (10) is similar to N_b, but excludes antiparallel pairs where plus ends are located opposite to each other.

We compute the three indices (8) in simulations to measure the combinations of filament mechanics, turnover, and model parameters that give rise to bundle formation. Similar to the time-averaged mean normal stress (7), we also compute the time-averaged indices

$$\overline{I_a} = \frac{1}{T}\int_0^T I_a(t)\, \mathrm{d}t, \quad (11)$$

$$\overline{I_b} = \frac{1}{T}\int_0^T I_b(t)\, \mathrm{d}t, \quad \text{and} \quad (12)$$

$$\overline{I_p} = \frac{1}{T}\int_0^T I_p(t)\, \mathrm{d}t. \quad (13)$$

Our indices provide general statistics to quantify bundle formation, and apply to simulations with different turnover methods and turnover rates. For example, the index I_b provides a useful single measure of overall bundle formation within a network, but does not explicitly identify individual bundles. One example of the random initial condition used in our simulations gave the baseline values $I_a = 0.1322$, $I_b = 0.0249$, and $I_p = 0.0130$. Throughout this work, we can consider an index elevated if the value of the index exceeds the baseline value. Using these indices, we focus on network-scale contractility and bundle formation, rather than measuring the contractility within individual bundles.

RESULTS

We obtain results for simulations with 150 filaments (each with equilibrium length of 1 μm) and 30 motors on a 5 μm × 5 μm domain, until $t = 300$ s using a time step size of $\Delta t = 0.05$ s. For each combination of parameters and turnover methods, we perform 10 simulations with a random initial condition. When reporting results, we denote quantities that are averaged across all simulations using angled bracket notation. For example, the trial-averaged mean normal stress is

$$\langle \sigma \rangle(t) = \frac{1}{N} \sum_{i=1}^{N} \sigma_i(t), \tag{14}$$

for each realization $\sigma_i(t)$ for $i = 1, \ldots N$, where $N = 10$. We denote time-averaged and trial-averaged quantities using both a bar and angled brackets. In subsequent sections, we often show results that are smoothed using a Savitzky-Golay filter, performed using the locally estimated scatterplot smoothing Julia package with span parameter $\alpha = 0.2$. Unless otherwise specified, parameters take the default values (4–6,12,21,23,51,54,57,60,66,76–84) indicated in the supporting material. Further explanation of these parameter values are provided in (23). Our key results are outlined below.

Trade-off between bundle formation and contractility

Our model reproduces the known result that networks without turnover lose contractility over time (11,23,85,86). Fig. 2 summarizes simulation results without turnover. Fig. 2 *A* displays the smoothed, time-averaged mean normal stress, showing that networks are initially contractile, but lose contractility after approximately $t = 100$ s to 150 s. Fig. 2 *B* shows that the aggregation, bundle formation, and parallel-bundle indices all increase initially, before reaching a plateau around the time that the network loses contractility. Increases in overall aggregation and bundle formation are largely explained by parallel-bundle formation, as myosin motors reorganize the network and draw filaments together. These parallel structures limit future contraction, because motors moving along two parallel filaments will not generate contraction (29). These results without turnover do not explain certain types of bundles that remain highly contractile, such as stress fibers, in which filaments form periodic structures and fibers' ends adhere to substrates. Our disordered networks lack both of these features. Instead, the key mechanism for generating contractility in our model is lateral filament bending (23), which is absent in the stress fibers.

Fig. 2 *C* shows the relationship between bundle index and stress, showing that networks with bundle indices $I_b < 0.1$ are contractile, but increased bundle formation leads to loss of contractility. The evolved network shown in Fig. 2 *D* illustrates that, after a period of initial contraction, distinct parallel structures form. These structures increase bundle formation but prevent sustained contractility. However, contractility also decreases if I_b is low (see Fig. 2 *C*), which can occur if filaments are not aggregated, reducing filament-filament interactions. This result suggests that an intermediate amount of bundle formation, approximately $I_b = 0.07$, is optimal for contractility. The amount of bundling that is optimal for contractility is two to three times the amount of bundling in the random initial condition, $I_b = 0.0249$. This optimal value of I_b depends on the number of filaments in the simulations, but not on the number of motors (see supporting material, section B.6 for details).

Uniform turnover prevents bundling and supports long-term contractility

Uniform turnover influences the trade-off between contractility and bundle formation by disrupting bundles, enabling prolonged contractility. This effect of uniform turnover has also been reported in previous studies (6,18,48,54). Fig. 3 summarizes the results for uniform turnover with rate $k_{\text{off},a} = 0.04\ \text{s}^{-1}$, a turnover rate estimated for cortical actomyosin networks (23). This value of $k_{\text{off},a}$ enables comparison with the no-turnover results in Fig. 2. Fig. 3 *A* shows that, with

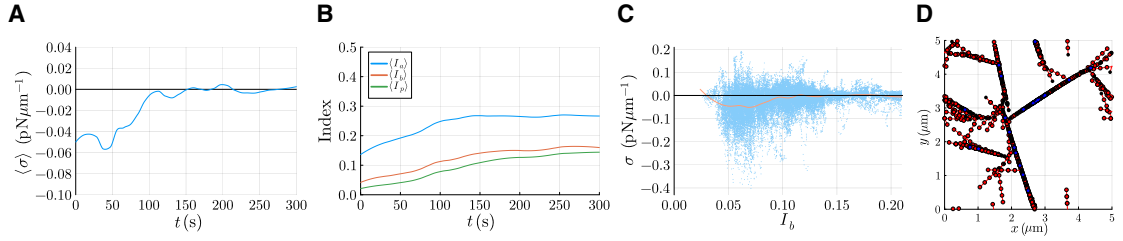

FIGURE 2 Numerical results for simulations with no turnover. (*A*) Trial-averaged mean normal stress over time for $N = 10$ simulations with no turnover, smoothed using a Savitzky-Golay filter (locally estimated scatterplot smoothing [LOESS] regression). (*B*) Trial-averaged bundle indices over time for $N = 10$ simulations with no turnover, smoothed using a Savitzky-Golay filter (LOESS regression). (*C*) Comparison of instantaneous measurements (*blue dots*) of mean normal stress and bundle index across all simulations and time. The solid curve is a LOESS regression of the data. (*D*) Example network configuration at $t = 300$ s. Red dots indicate F-actin nodes, red line segments indicate F-actin segments, black dots indicate F-actin plus ends, and blue dots indicate motor domains.

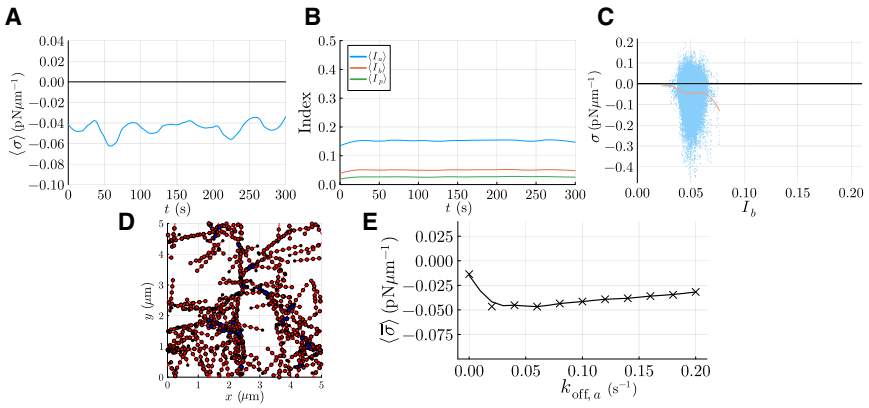

FIGURE 3 Numerical results for simulations with uniform turnover with rate $k_{\mathrm{off},a} = 0.04\ \mathrm{s}^{-1}$. (*A*) Trial-averaged mean normal stress over time for $N = 10$ simulations, smoothed using a Savitzky-Golay filter (LOESS regression). (*B*) Trial-averaged bundle indices over time for $N = 10$ simulations, smoothed using a Savitzky-Golay filter (LOESS regression). (*C*) Comparison of instantaneous measurements (*blue dots*) of mean normal stress and bundle index across all simulations and time. The solid curve is a LOESS regression of the data. (*D*) Example network configuration at $t = 300$ s. Red dots indicate F-actin nodes, red line segments indicate F-actin segments, black dots indicate F-actin plus ends, and blue dots indicate motor domains. (*E*) Relationship between uniform turnover rate and contractility. The solid curve is a LOESS regression of the data.

uniform turnover, the networks maintain contractility, with similar magnitude to the initial period of contraction of a disordered network. Fig. 3, *B* and *C*, suggest that prolonged contractility occurs because uniform turnover disrupts bundle formation. In Fig. 3 *B*, there is little change in the aggregation, bundle formation, or parallel-bundle formation indices over time. Fig. 3 *C* shows a similar relationship between bundle formation and contractility to Fig. 2 *C*, but due to turnover the amount of bundle formation never becomes sufficiently high to prevent contractility. Instead, I_b remains sufficiently low, within the range of values for I_b that Figs. 2 *C* and 3 *C* indicate are contractile. The evolved network in Fig. 3 *D* also does not exhibit the parallel-bundle formation that occurred without turnover (see Fig. 2 *D*), reinforcing the idea that uniform turnover disrupts parallel bundles. The experimental observation that contractile rings lose their force-generating abilities within minutes upon inhibition of the actin turnover (87) compares well with the model prediction that contractility in nondynamic networks is lost within 100–150 s.

In the fast-turnover rate limit, the network will approach the level of bundle formation associated with a random initial condition, $I_b \approx 0.0249$. This value of I_b is less than the amount of bundle formation that maximizes contractility, as shown in Fig. 2 *C* and reinforced in Fig. 3 *C*. Simulations with varying turnover rates suggest that there is an optimal uniform turnover rate lying between $k_{\mathrm{off},a} = 0.02\ \mathrm{s}^{-1}$ and $k_{\mathrm{off},a} = 0.06\ \mathrm{s}^{-1}$ that maximizes contractility. Interestingly, the turnover rate in cortical networks, $k_{\mathrm{off},a} \approx 0.04\mathrm{s}^{-1}$, is close to optimal for generating contraction in our simulations. The relationship between uniform turnover rate and contractility is shown in Fig. 3 *E*, and more detailed results are in the supporting material.

Biased turnover increases bundle formation and leads quickly to loss of contractility

Since the positions and orientations of new filaments depend on the existing network in the nonuniform turnover models, with nonuniform turnover the amount of filament reshuffling will be higher than that with no turnover, but less than with uniform turnover. In biased turnover, new filaments are placed close to existing filaments. As Fig. 4 *A* shows, contractility decreases quickly before $t = 50$ s, before settling in a seemingly steady state of weak contractility. Unlike the no-turnover scenario, the presence of turnover means that the network does not form stationary patterns and loses contractility completely. However, the spatial bias means that the contractility with biased turnover is much lower than the contractility with uniform turnover for the same turnover rate.

Fig. 4 *B* shows how biased turnover affects aggregation and bundle formation. All three indices, I_a, I_b, and I_p, increase over time. Compared with simulations with no turnover, biased turnover yields similar aggregation (I_a), but less bundle formation (I_b) and parallel-bundle formation (I_p). The trends in the bundle index, I_b, are consistent with the idea that contractility decreases as bundle formation increases. The relationship between I_b and σ shown in Fig. 4 *C*, which is similar to Fig. 2 *C*, reinforces this idea. With biased turnover, the bundle index stabilizes at $I_b \approx 0.1$, which is just low enough to maintain weak contractility.

With biased turnover, the difference $I_b - I_p$ also increases over time, suggesting an increase in antiparallel bundles. This trend is due to the possibility of polarity reversal in biased turnover and does not occur with no turnover or uniform turnover. Without turnover, the motors will instead pull filaments into stationary parallel arrangements. This difference is also reflected in the network patterns, as Fig. 4 *D* shows. The network with biased turnover forms a thicker aggregate, rather than a thin stationary pattern like those in Fig. 2 *D*. If polarity reversal is prevented, σ and I_b become more similar to the case of no turnover, with less contractility and more bundle formation. This is shown by the leftmost points in Fig. 4, *E* and *F*. Introducing even a small amount of polarity reversal, for example, $P_{\mathrm{rev}} = 0.1$, is sufficient to increase contractility and decrease bundle formation. Further details on the effects of parameter

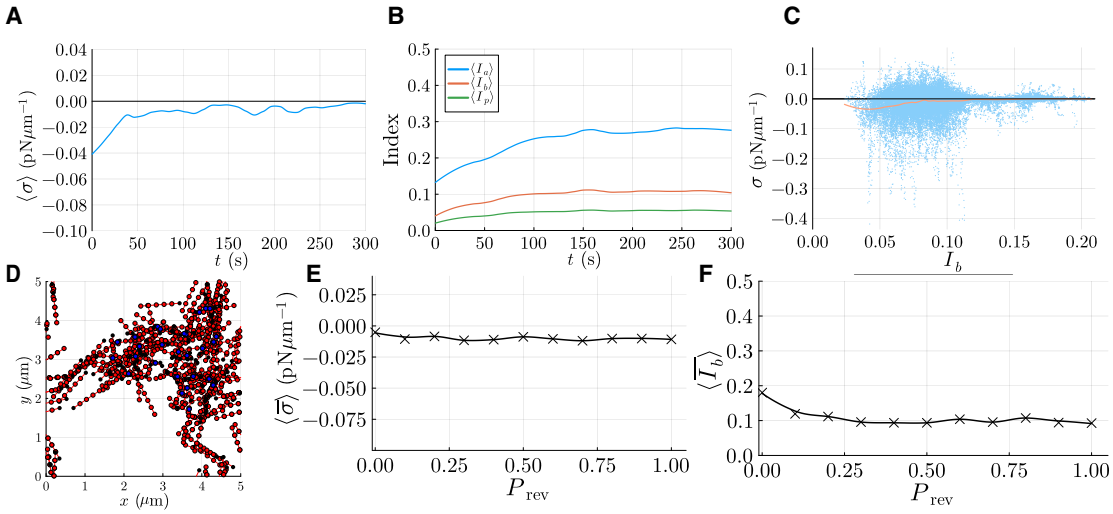

FIGURE 4 Numerical results for simulations with biased turnover with rate $k_{\text{off},a} = 0.04\ \text{s}^{-1}$. (*A*) Trial-averaged mean normal stress over time for $N = 10$ simulations, smoothed using a Savitzky-Golay filter (LOESS regression). (*B*) Trial-averaged bundle indices over time for $N = 10$ simulations, smoothed using a Savitzky-Golay filter (LOESS regression). (*C*) Comparison of instantaneous measurements (*blue dots*) of mean normal stress and bundle index across all simulations and time. The solid curve is a LOESS regression of the data. (*D*) Network configuration at $t = 300$ s. Red dots indicate F-actin nodes, red line segments indicate F-actin segments, black dots indicate F-actin plus ends, and blue dots indicate motor domains. (*E*) Impact of the polarity reversal probability, P_{rev}, on contractility. (*F*) Impact of the polarity reversal probability, P_{rev}, on bundle formation.

P_{rev}, and simulations exploring the effects of standard deviations $\sigma_{t,\theta}$, $\sigma_{t,x}$, and $\sigma_{t,y}$ are available in the supporting material, section B.2.

70° branching favors contractility over bundle formation

Fig. 5 shows how Arp2/3-mediated filament branching affects contractility and bundle formation. Like biased turnover, branched networks lose some contractility within the first 50 s, before settling at an approximately steady level of contractility (see Fig. 5 *A*). However, networks with branching turnover are more contractile than those with biased turnover. A possible explanation for this increased contractility is that branching is more effective than biased turnover at disrupting bundle formation. As Fig. 5 *B* shows, the amount of aggregation with branching is similar to biased turnover. The network snapshot in Fig. 5 *D* illustrates this result, where a filament aggregate forms on the right-hand side of the domain. However, branched networks maintain less overall bundle formation compared with biased turnover (see Fig. 5 *B*). This reduced bundling enables networks with branching to remain more contractile than networks with no turnover or biased turnover. However, branching remains less effective at promoting contractility than uniform turnover because the positions and orientations of new filaments exhibit spatial bias.

As Fig. 5, *E* and *F*, show, the angle $\theta_b = 70°$ is close to the optimal angle for maximizing contractility and decreasing aggregation, bundle formation, and parallel-bundle formation compared with other potential branching angles. Therefore, 70° branching appears to be a nonuniform turnover mechanism that disrupts bundles, favoring contractility over bundle formation. This finding reflects the results of Ennomani et al. (26), which experimentally support the higher contractility of branched networks.

Treadmilling promotes bundling while maintaining contractility

Unlike uniform turnover, biased turnover, and branching, treadmilling does not involve the removal and replacement of filaments in the network. Instead, existing filaments lose actin from their minus ends and gain actin at their plus ends, while not disappearing entirely. Fig. 6 *A* shows that treadmilling prevents the loss of contractility that occurs without turnover. Instead, the trend in contractility is similar to other nonuniform turnover methods, featuring a loss of contractility over the first approximately 50 s, before settling in a weakly contractile state. However, unlike biased turnover and branching, turnover with treadmilling in Fig. 6 *B* shows that aggregation, bundle formation, and parallel-bundle formation continue to increase over a longer time. The bundle formation index eventually reaches a similar value to that attained without turnover, suggesting that treadmilling must cause the persistent contractility observed in Fig. 6 *A*. The results in Fig. 6 *C*, where weaker contractility remains possible with larger values of I_b, reinforce this idea. Treadmilling lessens the negative feedback between bundle formation and contractility, enabling filaments within these bundles to retain net contractility.

The network configurations formed with treadmilling are also distinct from those formed with other turnover mechanisms. In Fig. 6 *D*, a long, thin curved filament bundle

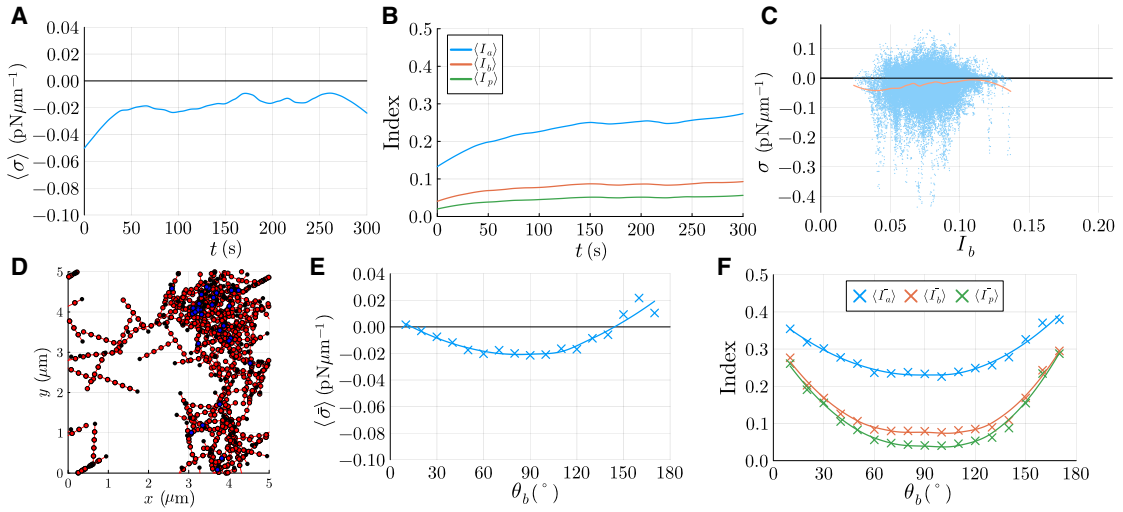

FIGURE 5 Numerical results for simulations with 70° branching turnover with rate $k_{\text{off},a} = 0.04\ \text{s}^{-1}$. (*A*) Trial-averaged mean normal stress over time for $N = 10$ simulations, smoothed using a Savitzky-Golay filter (LOESS regression). (*B*) Trial-averaged bundle indices over time for $N = 10$ simulations, smoothed using a Savitzky-Golay filter (LOESS regression). (*C*) Comparison of instantaneous measurements (*blue dots*) of mean normal stress and bundle index across all simulations and time. The solid curve is a LOESS regression of the data. (*D*) Example network configuration at $t = 300$ s. Red dots indicate F-actin nodes, red line segments indicate F-actin segments, black dots indicate F-actin plus ends, and blue dots indicate motor domains. (*E*) The effect of branching angle on time-averaged and trial-averaged stress. (*F*) The effect of branching angle on time-averaged and trial-averaged bundle indices. We performed $N = 10$ simulations for each value of θ_b (*crosses*), and smoothed using a Savitzky-Golay filter (*solid curves*).

reminiscent of an unattached stress fiber emerges in the upper part of the domain. Since most of the filament maintains its position during treadmilling, these patterns are similar to patterns without turnover (Fig. 2 *D*). Unlike the no turnover case, networks with treadmilling maintain contractility. Minus end disassembly provides a possible qualitative explanation for this persistent contractility (12). As the motors move toward filament plus ends, the minus ends are pushed apart, which could lead to expansion (29). The minus end disassembly diminishes this expansive potential, resulting in net contractility. Treadmilling may also cause the plus end and minus end locations to more closely resemble the periodic arrangement in contractile stress fibers (38,39).

Filament bending enhances bundle formation and protein friction enhances contractility for nonuniform turnover

Experimental studies found that actomyosin network contractility strongly depends on filament rigidity (88) and on mechanical resistance to deformations (26). Similarly, mechanical factors affect actin bundling (89). Thus, we conclude our investigation by exploring how flexural rigidity and the protein-friction coefficient affect contractility and bundle formation for each turnover model. Fig. 7 summarizes their effects. The background-drag coefficient and reference motor off-rate were less important (see supporting material for details), and we assumed the spring constants, free-moving motor velocity, and stall force to be fixed based on experimental data. These results agree with our previous study (23), where filament flexibility (reduced flexural rigidity) and protein friction promoted contractility.

Low flexural rigidity κ decreases resistance to filament bending. With uniform turnover, decreased κ increases network contractility until $\kappa = 0.02\,\text{pN}\,\mu\text{m}^2$, as Fig. 7 *A* shows. However, flexural rigidity has less impact on contractility for all methods of nonuniform turnover. Decreasing κ increases bundle formation (Fig. 7 *B*), because flexible filaments can more readily remodel into an aggregate due to myosin activity (see Fig. 7 *E*). These aggregates are less contractile than a disordered network due to the trade-off between bundle formation and contractility. Uniform turnover disrupts the aggregates and helps to maintain network contractility. In contrast, with nonuniform turnover the aggregates persist, because new filaments are more likely to emerge within the aggregate itself. As κ increases, branching and treadmilling disperse the aggregate more than biased turnover (see Fig. 7 *E*). Consequently, networks with branching and treadmilling yield networks that are more contractile compared with networks with biased turnover. However, although branching and treadmilling promote contractility more effectively than biased turnover, they are less effective than uniform turnover regardless of κ.

Increasing the protein-friction coefficient, λ_{pf}, increases contractility with all forms of turnover, as Fig. 7 *C* shows. Increasing λ_{pf} increases bundle formation for biased turnover and branching, as Fig. 7 *D* and the network snapshots shown in Fig. 7 *F* indicate. Since increasing λ_{pf} elevates both contractility and bundle formation with biased turnover and branching, strong protein friction (for example, due to cross-linking) may be important for generating persistent

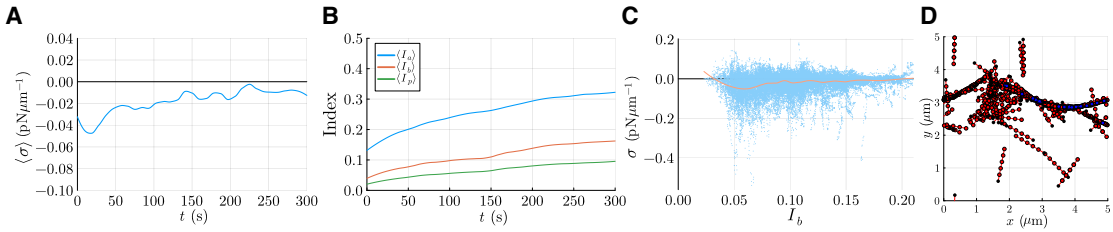

FIGURE 6 Numerical results for simulations with treadmilling turnover with rate $k_{\text{off},a} = 0.04\ \text{s}^{-1}$. (*A*) Trial-averaged mean normal stress over time for $N = 10$ simulations, smoothed using a Savitzky-Golay filter (LOESS regression). (*B*) Trial-averaged bundle indices over time for $N = 10$ simulations, smoothed using a Savitzky-Golay filter (LOESS regression). (*C*) Comparison of instantaneous measurements (*blue dots*) of mean normal stress and bundle index across all simulations and time. The solid curve is a LOESS regression of the data. (*D*) Example network configuration at $t = 300$ s. Red dots indicate F-actin nodes, red line segments indicate F-actin segments, black dots indicate F-actin plus ends, and blue dots indicate motor domains.

contractile bundles. With uniform turnover, I_b is largely independent of λ_{pf} because uniform turnover is effective at disrupting bundles regardless of λ_{pf}. With uniform turnover, there is large increase in contractility as λ_{pf} increases. In contrast, with biased turnover and branching, I_b increases as λ_{pf} increases. Due to the trade-off between bundle formation and contractility, this results in a smaller gain in contractility for these turnover methods as λ_{pf} increases, compared with uniform turnover.

For treadmilling turnover, increasing λ_{pf} decreases bundle formation, which is the opposite behavior to biased turnover and branching (see Fig. 7 *B*). When $\lambda_{\text{pf}} = 5$ pN μm^{-1} s (weak protein friction), networks with treadmilling form a very thin bundle (see Fig. 7 *F*) with high I_b. Small λ_{pf} corresponds to reduced resistance to relative motion between overlapping filaments, allowing the network to more easily remodel into the thin bundle structure, which resembles the stationary patterns produced with no turnover. With treadmilling, this pattern remains only weakly contractile. For low values of λ_{pf}, treadmilling yields less contractility than biased turnover or branching, due to the large discrepancy in I_b. As λ_{pf} increases, relative motion of overlapping filaments becomes more difficult, and the network with treadmilling remodels more slowly. For $\lambda_{\text{pf}} = 60$ pN μm^{-1} s, Fig. 7 *F* shows that the network no longer forms a single thin bundle. For treadmilling, this causes I_b to decrease as λ_{pf} increases. Contractility then increases with increasing λ_{pf}, due to both decreased bundle formation and the general contractile effect of protein friction. For large values of λ_{pf}, treadmilling yields increased contractility compared with biased turnover and branching. This increased contractility occurs despite the treadmilling networks maintaining I_b values similar to biased turnover networks for large λ_{pf}. The increased contractility with high I_b further reinforces the idea that treadmilling lessens the trade-off between bundle formation and contractility.

DISCUSSION AND CONCLUSION

In this work, we implemented an agent-based model of an actomyosin network with four turnover models: uniform, biased, branching, and treadmilling. We used the models to investigate the interplay between contractility, bundle formation, and turnover. Fig. 8 provides an overview of our results. Without turnover, there is negative feedback between bundle formation and contractility. Disordered networks initially contract, forming bundles. These bundles feature filaments aligned in parallel, similar to aster formation in previous studies (11,23,85,86). Eventually, these parallel structures become stationary, preventing further contractility. Uniform turnover, branching, and treadmilling can prolong contractility. Introducing uniform turnover or branching disrupts bundle formation, allowing network contractility to persist, whereas treadmilling disrupts the trade-off between bundle formation and continued contractility. In contrast, biased turnover increases bundle formation, which quickly results in reduced contractility. Mechanical factors also play a role in maintaining contractility and bundle formation. In our simulations, the clearest mechanical effects were that increased filament bending and protein friction promote contractility. Taken together, these results indicate that a combination of mechanically driven contractility and bundle-disrupting turnover is necessary to sustain network contractility and elevated bundle formation in initially disordered networks.

The most relevant previous computational study that examined the role of actin turnover on contractility of 3D networks in microscopic details (55) reached the same general conclusion that the moderate turnover enhances contractility. Macroscopic theory (90) posited the same point. Several other modeling studies explored the importance of turnover specifically in contractile rings (20,21), again concluding that dynamic actin is crucial for the maintenance of contractility. Two modeling studies found that not only steady but also pulsatile contractions depend on actin being dynamic (90,91). The advance our study offers is the comparison of several different modes of actin turnover.

In this study, we focused on isolating the effects of individual turnover models working alone. A realistic model for filament turnover in the cell might involve a combination of the turnover models that we investigated. Indeed, there are several subcellular processes in which different modes of

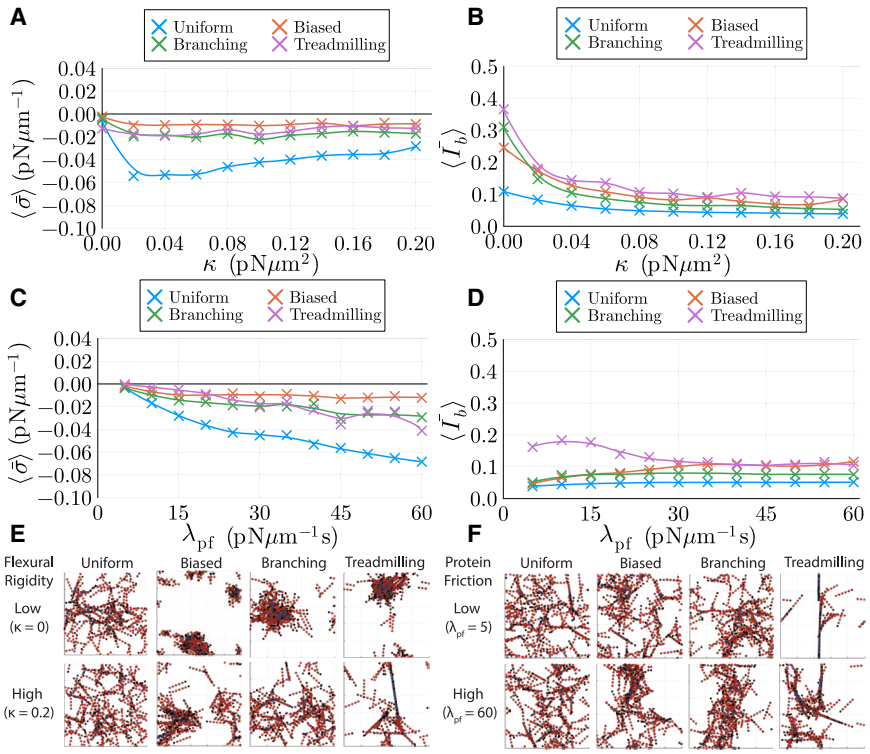

FIGURE 7 Numerical results for simulations with different forms of turnover with rate $k_{off,a} = 0.04\,s^{-1}$, and varying flexural rigidity κ and protein friction coefficient λ_{pf}. (*A*) The effect of κ on trial-averaged mean normal stress over time for $N = 10$ simulations (*crosses*). Solid curves are obtained by applying a Savitzky-Golay filter (LOESS regression). (*B*) The effect of κ on bundle formation index over time for $N = 10$ simulations (*crosses*). Solid curves are obtained by applying a Savitzky-Golay filter (LOESS regression). (*C*) The effect of λ_{pf} on trial-averaged mean normal stress over time for $N = 10$ simulations (*crosses*). Solid curves are obtained by applying a Savitzky-Golay filter (LOESS regression). (*D*) The effect of λ_{pf} on trial-averaged bundle formation index over time for $N = 10$ simulations (*crosses*). Solid curves are obtained by applying a Savitzky-Golay filter (LOESS regression). (*E*) The effect of flexural rigidity on network configuration at $t = 300\,s$ for different turnover models. Red dots indicate F-actin nodes, red line segments indicate F-actin segments, black dots indicate F-actin plus ends, and blue dots indicate motor domains. (*F*) The effect of protein-friction coefficient on network configuration for different turnover models.

filament turnover act in concert: two F-actin subpopulations (Arp2/3-governed shorter and more dynamic filaments interspersed with longer and more stable formin-associated filaments) with two different turnover kinetics were discovered in the cell actin cortex (92). Similarly, more dynamic branched lamellipodial networks coexist with more stable filopodial bundles at the cell leading edge (56). Another example is that different turnover modes coexist in the lamellipodia and lamellae of migrating epithelial cells (93). Related to that, our work suggests that some individual mechanisms have opposing effects on the trade-off between contractility and bundle formation. For example, uniform turnover and branching disrupt bundles and promote contractility, whereas biased turnover promotes bundle formation, hastening loss of contractility. A combination of turnover methods working in concert might allow cells to tune the levels of contractility and bundle formation, depending on the scenario. The rate of each turnover method might also influence this optimal combination. We present quantitative details on how the turnover rate, $k_{off,a}$, impacts contractility and bundle formation in the supporting material.

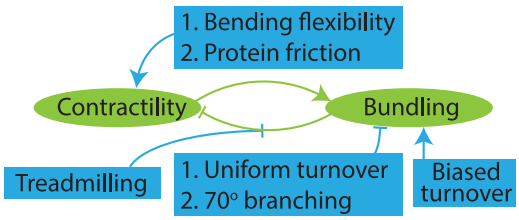

FIGURE 8 The interplay between contractility and bundling (*green ellipses*), and turnover methods and mechanical factors (*blue rectangles*) in initially disordered actomyosin networks. Lines between each group indicate the direction of causality. Arrow heads indicate factors that positively influence each other, and perpendicular lines indicate factors that negatively influence each other.

Several limitations of our approach must be considered when interpreting the results. Since the cell cortex is a thin layer, for simplicity we used a 2D model. Extending the model to 3D would require explicit simulation of motor and cross-linker binding and unbinding. 3D actomyosin networks look and behave differently (94) from the contractile cell cortex, but simulations suggest that actin turnover is as important in 3D (55) as it is in 2D. Our model neglects the complex modes of transport and turnover of motors and cross-linker proteins that occur in cells, and could redistribute stress and bundling. Pausing of motors on filament plus ends (95) could also significantly change the model predictions. Another limitation is that we do not compute localized forces and stress throughout the domain, but instead adopt a simplified model based on uniform deformation. Accounting for nonuniform directed and localized forces is a difficult problem beyond the scope of this study (96).

We also cannot rule out the possibility that domain size, filament concentration, and motor concentration might impact our results. We simulated hundreds of filaments and tens of motors in a 25 μm^2 domain. Judging by the

measured network mesh size (97), the number of filaments simulated is characteristic for the cell cortex. One (98) to tens (17) of myosin clusters per square μm were observed in the cortex, so our parameters are physiologically relevant, although the fact that there are multiple myosin molecules per cluster complicates the matter. Tam (23) showed that contractility is independent of domain size, provided that filament and motor concentrations are maintained. In the simulations of this paper, increasing the motor concentration increases contractility and bundle formation, but does not impact the qualitative effects of different turnover models illustrated in Fig. 8. These results are shown in the supporting material. The computational cost of the simulations constrains our ability to further verify the results on larger scales.

The filament turnover and mechanics investigated here could have potential implications for cell migration and division and tissue morphogenesis. Indeed, in cytokinesis, contractile ring action requires continuing actin turnover (87). Myosin and actin turnover are intimately intertwined in migrating cells (99). Actin turnover is crucial in effective contractility propagation between cells in tissue morphogenesis (94). To extend our model to these dynamic mechanochemical structures, one would have to introduce adhesions of actin to substrates and the membrane into the simulations.

DATA AND CODE AVAILABILITY

- Julia code and simulation results for varying turnover rates have been deposited on GitHub, and are publicly available at the URL https://github.com/alex-tam/ActomyosinBundle as of the article publication date.
- All other simulation results can be shared upon reasonable request.

ACKNOWLEDGMENTS

We acknowledge funding from the Australian Research Council (grant nos. DP180102956 and DE240100097). We also acknowledge Claudia Blom, whose summer research project informed the spatial statistics used in this work.

AUTHOR CONTRIBUTIONS

Conceptualization, A.K.Y.T., A.M., and D.B.O.; methodology, A.K.Y.T. and D.B.O.; software, A.K.Y.T.; analysis, A.K.Y.T. and D.B.O.; writing, A.K.Y.T. and A.M.; funding acquisition, D.B.O.

DECLARATION OF INTERESTS

The authors declare no competing interests.

SUPPORTING MATERIAL

Supporting material can be found online at https://doi.org/10.1016/j.bpj.2026.02.032.

REFERENCES

1. Pollard, T. D., and B. O'Shaughnessy. 2019. Molecular Mechanism of Cytokinesis. *Annu. Rev. Biochem.* 88:661–689. https://doi.org/10.1146/annurev-biochem-062917012530.
2. Yamada, K. M., and M. Sixt. 2019. Mechanisms of 3D Cell Migration. *Nat. Rev. Mol. Cell Biol.* 20:738–752. https://doi.org/10.1038/s41580-019-0172-9.
3. Chalut, K. J., and E. K. Paluch. 2016. The Actin Cortex: A Bridge between Cell Shape and Function. *Dev. Cell.* 38:571–573. https://doi.org/10.1016/j.devcel.2016.09.011.
4. Kamasaki, T., M. Osumi, and I. Mabuchi. 2007. Three-Dimensional Arrangement of F-actin in the Contractile Ring of Fission Yeast. *J. Cell Biol.* 178:765–771. https://doi.org/10.1083/jcb.200612018.
5. Dasanayake, N. L., P. J. Michalski, and A. E. Carlsson. 2011. General Mechanism of Actomyosin Contractility. *Phys. Rev. Lett.* 107:118101. https://doi.org/10.1103/PhysRevLett.107.118101.
6. Hiraiwa, T., and G. Salbreux. 2016. Role of Turnover in Active Stress Generation in a Filament Network. *Phys. Rev. Lett.* 116:188101. https://doi.org/10.1103/PhysRevLett.116.188101.
7. Huxley, H. E. 2004. Fifty Years of Muscle and the Sliding Filament Hypothesis. *Eur. J. Biochem.* 271:1403–1415. https://doi.org/10.1111/j.1432-1033.2004.04044.x.
8. Wachsstock, D. H., W. H. Schwarz, and T. D. Pollard. 1994. Cross-Linker Dynamics Determine the Mechanical Properties of Actin Gels. *Biophys. J.* 66:801–809. https://doi.org/10.1016/S0006-3495(94)80856-2.
9. Koenderink, G. H., and E. K. Paluch. 2018. Architecture Shapes Contractility in Actomyosin Networks. *Curr. Opin. Cell Biol.* 50:79–85. https://doi.org/10.1016/j.ceb.2018.01.015.
10. Yoshinaga, N., and P. Marcq. 2012. Contraction of Cross-Linked Actomyosin Bundles. *Phys. Biol.* 9:046004. https://doi.org/10.1088/1478-3975/9/4/046004.
11. Wang, S., and P. G. Wolynes. 2012. Active Contractility in Actomyosin Networks. *Proc. Natl. Acad. Sci. USA.* 109:6446–6451. https://doi.org/10.1073/pnas.1204205109.
12. Oelz, D. B., B. Y. Rubinstein, and A. Mogilner. 2015. A Combination of Actin Treadmilling and Cross-Linking Drives Contraction of Random Actomyosin Arrays. *Biophys. J.* 109:1818–1829. https://doi.org/10.1016/j.bpj.2015.09.013.
13. Gautel, M. 2011. The Sarcomeric Cytoskeleton: Who Picks up the Strain? *Curr. Opin. Cell Biol.* 23:39–46. https://doi.org/10.1016/j.ceb.2010.12.001.
14. Cramer, L. P., M. Siebert, and T. J. Mitchison. 1997. Identification of Novel Graded Polarity Actin Filament Bundles in Locomoting Heart Fibroblasts: Implications for the Generation of Motile Force. *J. Cell Biol.* 136:1287–1305. https://doi.org/10.1083/jcb.136.6.1287.
15. Hotulainen, P., and P. Lappalainen. 2006. Stress Fibers Are Generated by Two Distinct Actin Assembly Mechanisms in Motile Cells. *J. Cell Biol.* 173:383–394. https://doi.org/10.1083/jcb.200511093.
16. Pellegrin, S., and H. Mellor. 2007. Actin Stress Fibres. *J. Cell Sci.* 120:3491–3499. https://doi.org/10.1242/jcs.018473.
17. Chugh, P., A. G. Clark, …, E. K. Paluch. 2017. Actin Cortex Architecture Regulates Cell Surface Tension. *Nat. Cell Biol.* 19:689–697. https://doi.org/10.1038/ncb3525.
18. McFadden, W. M., P. M. McCall, …, E. M. Munro. 2017. Filament Turnover Tunes Both Force Generation and Dissipation to Control Long-Range Flows in a Model Actomyosin Cortex. *PLoS Comput. Biol.* 13:e1005811. https://doi.org/10.1371/journal.pcbi.1005811.
19. Rubinstein, B. Y., and A. Mogilner. 2017. Myosin Clusters of Finite Size Develop Contractile Stress in 1D Random Actin Arrays. *Biophys. J.* 113:937–947. https://doi.org/10.1016/j.bpj.2017.07.003.
20. Mendes Pinto, I., B. Rubinstein, …, R. Li. 2012. Actin Depolymerization Drives Actomyosin Ring Contraction during Budding Yeast Cytokinesis. *Dev. Cell.* 22:1247–1260. https://doi.org/10.1016/j.devcel.2012.04.015.

21. Stachowiak, M. R., C. Laplante, …, B. O'Shaughnessy. 2014. Mechanism of Cytokinetic Contractile Ring Constriction in Fission Yeast. *Dev. Cell.* 29:547–561. https://doi.org/10.1016/j.devcel.2014.04.021.

22. Kim, T. 2015. Determinants of Contractile Forces Generated in Disorganized Actomyosin Bundles. *Biomech. Model. Mechanobiol.* 14:345–355. https://doi.org/10.1007/s10237-014-0608-2.

23. Tam, A. K. Y., A. Mogilner, and D. B. Oelz. 2021. Protein Friction and Filament Bending Facilitate Contraction of Disordered Actomyosin Networks. *Biophys. J.* 120:4029–4040. https://doi.org/10.1016/j.bpj.2021.08.012.

24. Head, D. A., A. J. Levine, and F. C. MacKintosh. 2003. Distinct Regimes of Elastic Response and Deformation Modes of Cross-Linked Cytoskeletal and Semiflexible Polymer Networks. *Phys. Rev. E.* 68:061907. https://doi.org/10.1103/PhysRevE.68.061907.

25. Murrell, M., P. W. Oakes, …, M. L. Gardel. 2015. Forcing Cells into Shape: The Mechanics of Actomyosin Contractility. *Nat. Rev. Mol. Cell Biol.* 16:486–498. https://doi.org/10.1038/nrm4012.

26. Ennomani, H., G. Letort, …, L. Blanchoin. 2016. Architecture and Connectivity Govern Actin Network Contractility. *Curr. Biol.* 26:616–626. https://doi.org/10.1016/j.cub.2015.12.069.

27. Lenz, M. 2014. Geometrical Origins of Contractility in Disordered Actomyosin Networks. *Phys. Rev. X.* 4:041002. https://doi.org/10.1103/PhysRevX.4.041002.

28. Komianos, J. E., and G. A. Papoian. 2018. Stochastic Ratcheting on a Funneled Energy Landscape Is Necessary for Highly Efficient Contractility of Actomyosin Force Diploes. *Phys. Rev. X.* 8:021006. https://doi.org/10.1103/PhysRevX.8.021006.

29. Tam, A. K. Y., A. Mogilner, and D. B. Oelz. 2022. F-Actin Bending Facilitates Net Actomyosin Contraction by Inhibiting Expansion with plus-End-Located Myosin Motors. *J. Math. Biol.* 85:4. https://doi.org/10.1007/s00285-022-01737-z.

30. Belmonte, J. M., M. Leptin, and F. Nédélec. 2017. A Theory That Predicts Behaviors of Disordered Cytoskeletal Networks. *Mol. Syst. Biol.* 13:941. https://doi.org/10.15252/msb.20177796.

31. Lenz, M., M. L. Gardel, and A. R. Dinner. 2012. Requirements for Contractility in Disordered Cytoskeletal Bundles. *New J. Phys.* 14:033037. https://doi.org/10.1088/1367-2630/14/3/033037.

32. Lenz, M., T. Thoresen, …, A. R. Dinner. 2012. Contractile Units in Disordered Actomyosin Bundles Arise from F-actin Buckling. *Phys. Rev. Lett.* 108:238107. https://doi.org/10.1103/PhysRevLett.108.238107.

33. Cortes, D. B., M. Gordon, …, A. S. Maddox. 2020. Bond Type and Discretization of Nonmuscle Myosin II Are Critical for Simulated Contractile Dynamics. *Biophys. J.* 118:2703–2717. https://doi.org/10.1016/j.bpj.2020.03.033.

34. Matsuda, K., W. Jung, …, J. Yajima. 2024. Myosin-Induced F-actin Fragmentation Facilitates Contraction of Actin Networks. *Cytoskeleton.* 81:339–355. https://doi.org/10.1002/cm.21848.

35. Nédélec, F. J., and D. Foethke. 2007. Collective Langevin Dynamics of Flexible Cytoskeletal Fibers. *New J. Phys.* 9:427. https://doi.org/10.1088/1367-2630/9/11/427.

36. Freedman, S. L., S. Banerjee, …, A. R. Dinner. 2017. A Versatile Framework for Simulating the Dynamic Mechanical Structure of Cytoskeletal Networks. *Biophys. J.* 113:448–460. https://doi.org/10.1016/j.bpj.2017.06.003.

37. Popov, K., J. Komianos, and G. A. Papoian. 2016. MEDYAN: Mechanochemical Simulations of Contraction and Polarity Alignment in Actomyosin Networks. *PLoS Comput. Biol.* 12:e1004877. https://doi.org/10.1371/journal.pcbi.1004877.

38. Kolley, F., C. Sidor, …, B. M. Friedrich. 2024. Mechanisms of Sarcomere Assembly in Muscle Cells Inferred from Sequential Ordering of Myofibril Components. *PRX Life.* 2:013002. https://doi.org/10.1103/PRXLife.2.013002.

39. Mao, Q., A. Acharya, …, F. Schnorrer. 2022. Tension-Driven Multi-Scale Self-Organisation in Human iPSC-derived Muscle Fibers. *eLife.* 11:e76649. https://doi.org/10.7554/eLife.76649.

40. Lenz, M. 2020. Reversal of Contractility as a Signature of Self-Organization in Cytoskeletal Bundles. *eLife.* 9:e51751. https://doi.org/10.7554/eLife.51751.

41. Vavylonis, D., J. Q. Wu, …, T. D. Pollard. 2008. Assembly Mechanism of the Contractile Ring for Cytokinesis by Fission Yeast. *Science.* 319:97–100. https://doi.org/10.1126/science.1151086.

42. Maxian, O., A. Donev, and A. Mogilner. 2022. Interplay between Brownian Motion and Cross-Linking Controls Bundling Dynamics in Actin Networks. *Biophys. J.* 121:1230–1245. https://doi.org/10.1016/j.bpj.2022.02.030.

43. Zilman, A. G., and S. A. Safran. 2003. Role of Cross-Links in Bundle Formation, Phase Separation and Gelation of Long Filaments. *EPL.* 63:139–145. https://doi.org/10.1209/epl/i2003-00489-5.

44. Kierfeld, J., T. Kühne, and R. Lipowsky. 2005. Discontinuous Unbinding Transitions of Filament Bundles. *Phys. Rev. Lett.* 95:038102. https://doi.org/10.1103/PhysRevLett.95.038102.

45. Meyer, R. K., and U. Aebi. 1990. Bundling of Actin Filaments by Alpha-Actinin Depends on Its Molecular Length. *J. Cell Biol.* 110:2013–2024. https://doi.org/10.1083/jcb.110.6.2013.

46. Freedman, S. L., C. Suarez, …, G. M. Hocky. 2019. Mechanical and Kinetic Factors Drive Sorting of F-actin Cross-Linkers on Bundles. *Proc. Natl. Acad. Sci. USA.* 116:16192–16197. https://doi.org/10.1073/pnas.1820814116.

47. Bidone, T. C., W. Jung, …, T. Kim. 2017. Morphological Transformation and Force Generation of Active Cytoskeletal Networks. *PLoS Comput. Biol.* 13:e1005277. https://doi.org/10.1371/journal.pcbi.1005277.

48. Tang, H., D. Laporte, and D. Vavylonis. 2014. Actin Cable Distribution and Dynamics Arising from Cross-Linking, Motor Pulling, and Filament Turnover. *Mol. Biol. Cell.* 25:3006–3016. https://doi.org/10.1091/mbc.E14-05-0965.

49. Chandrasekaran, A., A. Upadhyaya, and G. A. Papoian. 2019. Remarkable Structural Transformations of Actin Bundles Are Driven by Their Initial Polarity, Motor Activity, Crosslinking, and Filament Treadmilling. *PLoS Comput. Biol.* 15:e1007156. https://doi.org/10.1371/journal.pcbi.1007156.

50. Reymann, A. C., J. L. Martiel, …, M. Théry. 2010. Nucleation Geometry Governs Ordered Actin Networks Structures. *Nat. Mater.* 9:827–832. https://doi.org/10.1038/nmat2855.

51. Thoresen, T., M. Lenz, and M. L. Gardel. 2011. Reconstitution of Contractile Actomyosin Bundles. *Biophys. J.* 100:2698–2705. https://doi.org/10.1016/j.bpj.2011.04.031.

52. Ciocanel, M.-V., A. Chandrasekaran, …, A. Dawes. 2022. Simulated Actin Reorganization Mediated by Motor Proteins. *PLoS Comput. Biol.* 18:e1010026. https://doi.org/10.1371/journal.pcbi.1010026.

53. González-Tokman, C., and D. B. Oelz. 2024. Asymptotic Limits of Transient Patterns in a Continuous-Space Interacting Particle System. *Proc. Royal Soc. A.* 480:20230754. https://doi.org/10.1098/rspa.2023.0754.

54. Zumdieck, A., K. Kruse, …, F. Jülicher. 2007. Stress Generation and Filament Turnover during Actin Ring Constriction. *PLoS One.* 2:e696. https://doi.org/10.1371/journal.pone.0000696.

55. Mak, M., M. H. Zaman, …, T. Kim. 2016. Interplay of Active Processes Modulates Tension and Drives Phase Transition in Self-Renewing, Motor-Driven Cytoskeletal Networks. *Nat. Commun.* 7:10323. https://doi.org/10.1038/ncomms10323.

56. Goode, B. L., J. Eskin, and S. Shekhar. 2023. Mechanisms of Actin Disassembly and Turnover. *J. Cell Biol.* 222:e202309021. https://doi.org/10.1083/jcb.202309021.

57. Gittes, F., B. Mickey, …, J. Howard. 1993. Flexural Rigidity of Microtubules and Actin Filaments Measured from Thermal Fluctuations in Shape. *J. Cell Biol.* 120:923–934. https://doi.org/10.1083/jcb.120.4.923.

58. Letort, G., A. Z. Politi, …, L. Blanchoin. 2015. Geometrical and Mechanical Properties Control Actin Filament Organization. *PLoS Comput. Biol.* 11:e1004245. https://doi.org/10.1371/journal.pcbi.1004245.

59. Bell, G. I. 1978. Models for the Specific Adhesion of Cells to Cells. *Science.* 200:618–627. https://doi.org/10.1126/science.347575.

60. Ward, A., F. Hilitski, …, Z. Dogic. 2015. Solid Friction between Soft Filaments. *Nat. Mater.* 14:583–588. https://doi.org/10.1038/nmat4222.

61. Lin, S., X. Han, …, L. Gu. 2017. Active Stiffening of F-actin Network Dominated by Structural Transition of Actin Filaments into Bundles. *Compos. B Eng.* 116:377–381. https://doi.org/10.1016/j.compositesb.2016.10.079.

62. Andrianantoandro, E., and T. D. Pollard. 2006. Mechanism of Actin Filament Turnover by Severing and Nucleation at Different Concentrations of ADF/Cofilin. *Mol. Cell.* 24:13–23. https://doi.org/10.1016/j.molcel.2006.08.006.

63. Murrell, M. P., and M. L. Gardel. 2012. F-Actin Buckling Coordinates Contractility and Severing in Biomimetic Actomyosin Cortex. *Proc. Natl. Acad. Sci. USA.* 109:20820–20825. https://doi.org/10.1073/pnas.1214753109.

64. Maciver, S. K., and P. J. Hussey. 2002. The ADF/Cofilin Family: Actin-Remodeling Proteins. *Genome Biol.* 3:reviews3007. https://doi.org/10.1186/gb-2002-3-5-reviews3007.

65. Southwick, F. S. 2000. Gelsolin and ADF/Cofilin Enhance the Actin Dynamics of Motile Cells. *Proc. Natl. Acad. Sci. USA.* 97:6936–6938. https://doi.org/10.1073/pnas.97.13.6936.

66. Mullins, R. D., J. A. Heuser, and T. D. Pollard. 1998. The Interaction of Arp2/3 Complex with Actin: Nucleation, High Affinity Pointed End Capping, and Formation of Branching Networks of Filaments. *Proc. Natl. Acad. Sci. USA.* 95:6181–6186. https://doi.org/10.1073/pnas.95.11.6181.

67. Woodrum, D. T., S. A. Rich, and T. D. Pollard. 1975. Evidence for Biased Bidirectional Polymerization of Actin Filaments Using Heavy Meromyosin Prepared by an Improved Method. *J. Cell Biol.* 67:231–237. https://doi.org/10.1083/jcb.67.1.231.

68. Svitkina, T. 2018. The Actin Cytoskeleton and Actin-Based Motility. *Cold Spring Harb. Perspect. Biol.* 10:a018267. https://doi.org/10.1101/cshperspect.a018267.

69. Svitkina, T. M. 2018. Ultrastructure of the Actin Cytoskeleton. *Curr. Opin. Cell Biol.* 54:1–8. https://doi.org/10.1016/j.ceb.2018.02.007.

70. Arroyo, M., N. Walani, …, D. Kaurin. 2018. Onsager's Variational Principle in Soft Matter: Introduction and Application to the Dynamics of Adsorption of Proteins onto Fluid Membranes. *In* The Role of Mechanics in the Study of Lipid Bilayers, CISM International Centre for Mechanical Sciences, *11*. D. J. Steigmann, ed. Springer International Publishing, pp. 287–332.

71. Broyden, C. G. 1970. The Convergence of a Class of Double-Rank Minimization Algorithms 1. General Considerations. *IMA J. Appl. Math.* 6:76–90. https://doi.org/10.1093/imamat/6.1.76.

72. Fletcher, R. 1970. A New Approach to Variable Metric Algorithms. *Comput. J.* 13:317–322. https://doi.org/10.1093/comjnl/13.3.317.

73. Goldfarb, D. 1970. A Family of Variable-Metric Methods Derived by Variational Means. *Math. Comp.* 24:23–26. https://doi.org/10.1090/S0025-5718-1970-0258249-6.

74. Shanno, D. F. 1970. Conditioning of Quasi-Newton Methods for Function Minimization. *Math. Comp.* 24:647–656. https://doi.org/10.1090/S0025-5718-1970-0274029-X.

75. Mogensen, P. K., and A. N. Risbeth. 2018. Optim: A Mathematical Optimization Package for Julia. *J. Open Source Softw.* 3:615. https://doi.org/10.21105/joss.00615.

76. Berg, H. C. 1993. Random Walks in Biology. Princeton University Press.

77. Oelz, D. B., U. Del Castillo, …, A. Mogilner. 2018. Microtubule Dynamics, Kinesin-1 Sliding, and Dynein Action Drive Growth of Cell Processes. *Biophys. J.* 115:1614–1624. https://doi.org/10.1016/j.bpj.2018.08.046.

78. Kim, T., M. L. Gardel, and E. Munro. 2014. Determinants of Fluidlike Behaviour and Effective Viscosity in Cross-Linked Actin Networks. *Biophys. J.* 106:526–534. https://doi.org/10.1016/j.bpj.2013.12.031.

79. Reichl, E. M., Y. Ren, …, D. N. Robinson. 2008. Interactions between Myosin and Actin Crosslinkers Control Cytokinesis Contractility Dynamics and Mechanics. *Curr. Biol.* 18:471–480. https://doi.org/10.1016/j.cub.2008.02.056.

80. Wu, J. Q., and T. D. Pollard. 2005. Counting Cytokinesis Proteins Globally and Locally in Fission Yeast. *Science.* 310:310–314. https://doi.org/10.1126/science.1113230.

81. Saha, A., M. Nishikawa, …, S. W. Grill. 2016. Determining Physical Properties of the Cell Cortex. *Biophys. J.* 110:1421–1429. https://doi.org/10.1016/j.bpj.2016.02.013.

82. Stam, S., J. Alberts, …, E. Munro. 2015. Isoforms Confer Characteristic Force Generation and Mechanosensation by Myosin II Filaments. *Biophys. J.* 108:1997–2006. https://doi.org/10.1016/j.bpj.2015.03.030.

83. Wang, F., M. Kovacs, …, J. R. Sellers. 2003. Kinetic Mechanism of Non-Muscle Myosin IIB. *J. Biol. Chem.* 278:27439–27448. https://doi.org/10.1074/jbc.M302510200.

84. Erdmann, T., and U. S. Schwarz. 2012. Stochastic Force Generation by Small Ensembles of Myosin II Motors. *Phys. Rev. Lett.* 108:188101. https://doi.org/10.1103/PhysRevLett.108.188101.

85. Gordon, D., A. Bernheim-Groswasser, …, O. Farago. 2012. Hierarchical Self-Organization of Cytoskeletal Active Networks. *Phys. Biol.* 9:026005. https://doi.org/10.1088/1478-3975/9/2/026005.

86. Nédélec, F. J. 1997. Self-Organisation of Microtubules and Motors. *Nature.* 389:305–308. https://doi.org/10.1038/38532.

87. Chew, T. G., J. Huang, …, M. K. Balasubramanian. 2017. Actin turnover maintains actin filament homeostasis during cytokinetic ring contraction. *J. Cell Biol.* 216:2657–2667.

88. Stam, S., S. L. Freedman, …, M. L. Gardel. 2017. Filament rigidity and connectivity tune the deformation modes of active biopolymer networks. *Proc. Natl. Acad. Sci. USA.* 114:E10037–E10045.

89. Freedman, S. L., G. M. Hocky, …, A. R. Dinner. 2018. Nonequilibrium Phase Diagrams for Actomyosin Networks. *Soft Matter.* 14:7740–7747. https://doi.org/10.1039/c8sm00741a.

90. Banerjee, D. S., A. Munjal, …, M. Rao. 2017. Actomyosin pulsation and flows in an active elastomer with turnover and network remodeling. *Nat. Commun.* 8:1121.

91. Yu, Q., J. Li, …, T. Kim. 2018. Balance between Force Generation and Relaxation Leads to Pulsed Contraction of Actomyosin Networks. *Biophys. J.* 115:2003–2013. https://doi.org/10.1016/j.bpj.2018.10.008.

92. Fritzsche, M., A. Lewalle, …, G. Charras. 2013. Analysis of turnover dynamics of the submembranous actin cortex. *Mol. Biol. Cell.* 24:757–767.

93. Ponti, A., A. Matov, …, G. Danuser. 2005. Periodic patterns of actin turnover in lamellipodia and lamellae of migrating epithelial cells analyzed by quantitative Fluorescent Speckle Microscopy. *Biophys. J.* 89:3456–3469.

94. Heer, N. C., and A. C. Martin. 2017. Tension, contraction and tissue morphogenesis. *Development.* 144:4249–4260.

95. Wollrab, V., J. M. Belmonte, …, G. H. Koenderink. 2018. Polarity Sorting Drives Remodeling of Actin-Myosin Networks. *J. Cell Sci.* 132:jcs219717. https://doi.org/10.1242/jcs.219717.

96. Goriely, A. 2017. The Mathematics and Mechanics of Biological Growth. *In* Interdisciplinary Applied Mathematics, *45* Springer.

97. Svitkina, T. M. 2020. Actin Cell Cortex: Structure and Molecular Organization. *Trends Cell Biol.* 30:556–565. https://doi.org/10.1016/j.tcb.2020.03.005.

98. Linsmeier, I., S. Banerjee, …, M. P. Murrell. 2016. Disordered actomyosin networks are sufficient to produce cooperative and telescopic contractility. *Nat. Commun.* 7:12615.

99. Chandra, A., M. T. Butler, …, J. M. Haugh. 2022. Modeling cell protrusion predicts how myosin II and actin turnover affect adhesion-based signaling. *Biophys. J.* 121:102–118.